A Color Model for Digital Photo Printing on Silver Halide Paper

Roland Meier and Peter Zolliker
GRETAG IMAGING AG
Regensdorf, Switzerland

Abstract

Today's digital photo-finishing equipment support various input and output devices. In these systems the color management is essential and can greatly benefit from a paper model that predicts the color behavior of silver halide paper.

Negative film is an important input channel for most digital minilabs, such as Master*flex*D or Cyra system from Gretag Imaging AG. Typically, a negative film is scanned and digitized. A color-matching algorithm generates normalized, film-independent, and mask-corrected film densities (*e.g.* EyeTech). As opposed to analogue laboratories the exposing unit of a digital photo printer does not expose paper through negative film. Instead, normalized film densities are converted to CIELAB colors of an ideal paper using a spectral paper model. From the 'device-independent' CIELAB color space the image is mapped to the appropriate output device. In Master*flex*D and Cyra*fast*print a common output device is the digital photo-printer using DMD technology. The assumption of an ideal paper prevents us from restricting the gamut of the 'device-independent' CIELAB color space to a particular paper brand. The out-of-gamut areas between the 'device-independent' color space, the final print, and the sRGB monitor are kept small to minimize losses in image quality during gamut mapping.

The color model is also useful at the output. For output profiling classical color management tools use measured tristimuli from a large set of colored patches to probe the gamut and to relate CIELAB color values to the corresponding printer RGB values. A spectral model helps drastically reduce the number of required colored patches. In addition, a spectral model facilitates the description of the gamut boundaries compared to a purely empirical, grid-interpolating method.

Introduction

Every imaging system has to employ some kind of color management (CM) to control and modify the color information of images that are processed through the system (*cf* Giorgianni and Madden[1]). The color gamut, the spatial resolving power, or the signal-to-noise ratio are a few examples of intrinsic physical limitations any image capturing or reproduction system has to cope with. But even if we manage to obtain a perfect colorimetric match of a live scene, experience tells us that the overall appearance of the reproduced image is still unsatisfactory as long as perceptual effects are neglected. The observer automatically adapts to the general brightness of the image and its immediate environment. Chromatic adaptation leads to a shift of the white point. Color memory effects and lateral brightness adaptation are other factors that have an impact on human perception.

The focus of this paper is on signal processing between negative film and printout on silver halide paper. Over the course of a century, several generations of photo-chemists optimized the analogue transformation from the original scene to the negative film, and from thereon to photographic paper. Since conventional photography has learned to overcome the various CM problems, it is reasonable to mimic the analogue system as closely as possible. We carefully model the analogue data path connecting negative film and photographic paper. Major attention is paid to the modeling of silver-halide paper and the benefits of using such a model.

Color Management

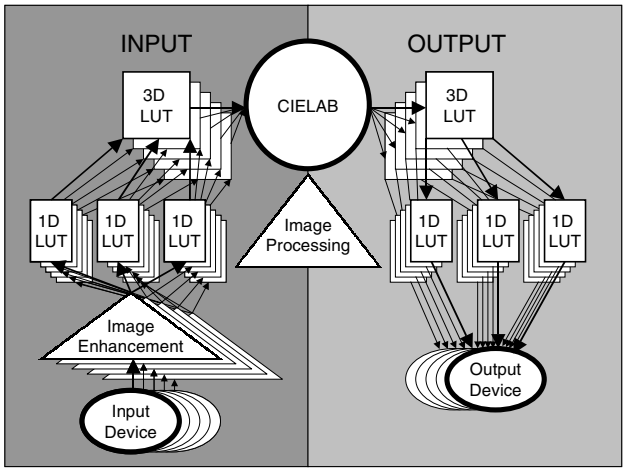

Figure 1. Schematic view of the color management in MasterflexD and Cyra system.

Today's digital minilabs handle a number of different input and output devices (Fig. 1). For example the digital minilab Master*flex*D from Gretag Imaging AG receives data from a negative film scanner, a flatbed scanner, a third-party slide scanner, and different digital input media such as Zip, CD, internet, CompactFlash and

SmartMedia cards from digital cameras, *etc*. The output is sent to a digital printer equipped with a 1280 pixel wide DMD array (Digital Mirroring Device), to the CRT (Cathode Ray Tube) screen for the operator, or to one of the numerous digital output devices.

The 'device independent', common CIELAB color space (circle in Fig. 1), used as profile connection space, plays a central role in our color management strategy. Data captured by a particular input device are optimized in the original coordinate system of the device. Thereafter the images are transformed to CIELAB triplets using three 1D LUTs (look-up tables) followed by a 3D LUT with 65^3 grid points. At the output the order of the LUTs is reversed to map the CIELAB values to the corresponding color coordinates of the destination device. The strict separation between input and output channels allows us to exclusively focus on the transformations from or to the profile connection space, whenever a new device is added to the system. Without this central color space a transformation had to be introduced for every input-output combination. The central profile connection space is the natural place to perform common, device-independent image processing.

The CIELAB color space offers a number of important advantages over other data coordinate systems such as sRGB. Lightness L is completely separated from the (a, b)-color plane. The metric of the CIELAB color space is adapted to the perception of the eye. Optimal color encoding is close to linear in Lab coordinates. The gamut is virtually unrestricted. The sRGB to CIELAB conversion and the inverse can be described by piecewise analytical functions. Somewhat unfortunate is the fact that the CIELAB color space is little known to the consumer market. Note that the various transformations to the profile connection space do not necessarily map to the same gamut. Quite often the gamut of an image in the CIELAB color space reveals the source device. In this sense the common CIELAB color space is not really 'device-independent'.

The Data Path from Negative Film Scanner to Digital Photographic Printer

A basic block diagram of the data flow from negative film to the printout of the DMD printer is depicted in Fig. 2. The scanner delivers calibrated, though unprocessed RGB densities $\boldsymbol{d}_{\text{scan}}$ of the negative film. Gretag employs the EyeTech algorithm (Marbach *et al*. [2]) to remove the film mask, to determine the gray-axis, to compensate for scene-dependent illumination effects, to adjust under- and overexposed images, and to convert to film-independent, normalized, RGB film densities $\boldsymbol{d}_{\text{film}}$.

$$\boldsymbol{d}_{\text{film}} = \boldsymbol{A}\,\boldsymbol{d}_{\text{scan}} + \boldsymbol{t}\,, \tag{1}$$

where $\boldsymbol{A}$ is a 3×3 matrix and $\boldsymbol{t}$ an RGB-vector of dimension 3. An additional set of filters is used to do image enhancement in the space of film densities. In an analogue system the 3 exposure times are the only adjustable parameters. In the digital case we have a higher degree of freedom. We try to model the transition from film densities $\boldsymbol{d}_{\text{film}}$ of an 'ideal film' to CIELAB values of an 'ideal paper'. For this purpose we introduce a two-step simulation of the film-paper system:

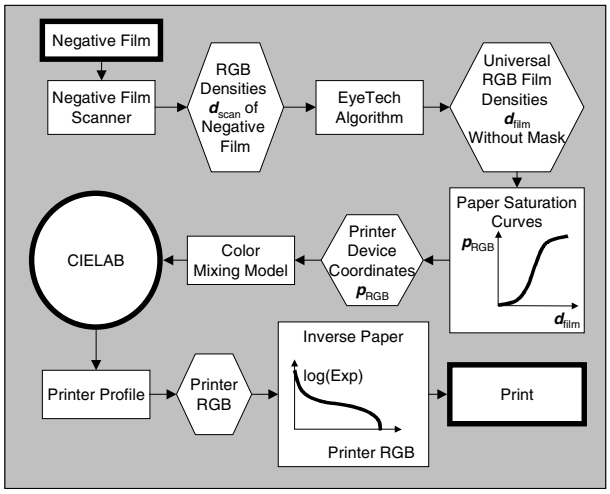

Figure 2. Data path between the scanner for negative film and the digital photographic printer.

Step 1: Transformation from d_{film} to normalized device coordinates RGB p_{RGB} of the printer

Let's assume a light source illuminates an ideal film through three narrow-band filters in R, G, and B. In an approximation of first order the R, G, and B images excite the respective yellow (Y), magenta (M), or cyan (C) dye-forming layer of the photographic paper. The flanks of the dye sensitivity-curves may extend into neighboring excitation channels and lead to cross-excitations. Those are treated with a linear 3×3 matrix $\boldsymbol{C}$. For the DMD printer with paper densities ranging from 0 to ~2.3 we can safely set $\boldsymbol{C} = \boldsymbol{1}$. The response of the dye-forming layers to light is non-linear and can be approximated by, for example, *tanh*-shaped curves. It is possible to use more sophisticated approximations for the paper saturation curves (Zolliker[3]). The saturation curves compress the image near low and high densities. They are a desired property of photographic paper and produce an optimal gray-axis for typical images. The saturation curves convert the incoming RGB film densities $\boldsymbol{d}_{\text{film}}$ to [0, 1] normalized device coordinates $\boldsymbol{p}_{\text{RGB}}$. The printer has to be gray-calibrated, and both steps 1 and 2 of the model shall not modify the gray-axis. Obviously at the input of the film-paper path the three *tanh*-shaped 1D LUTs for the R, G, and B channel ought to be identical.

Step 2: Transformation from Device Coordinates p_{RGB} to CIELAB Values of Silver-Halide Paper

RGB device coordinates of the printer with $R = G = B = \xi$ are expected to print gray colors with a CIELAB value of L proportional to ξ. It is the task of the gray calibration to guarantee this proportionality on the gray axis. For all other RGB printer coordinates a spectral model predicts the appropriate CIELAB triplet. At the input the model requires CMY dye concentrations $c_i \in [0, 1]$ for primary dyes $i = 1, \ldots, n$. The return values are CIELAB triplets of the print. In principle concentrations c_i could also be larger than 1. The transformation is stored in a 65^3 3D LUT. The resulting CIELAB values are fed to the profile connection space, from where the data can be processed to an arbitrary output device *via* conventional

profiling. CMY dye concentrations c_i are derived from RGB device coordinates $\boldsymbol{p}_{\mathrm{RGB}}$.

A Simple Spectral Paper Model

A uniform layer of colored gel on top of a solid, white substratum is a simple model of photographic (silver-halide) paper. In the gel continuous tone color mixing is achieved by adding a homogenous mixture of n primary dyes. The Kubelka-Munk approach assumes light can only travel in two directions perpendicular to the colored gel layer: Upward with intensity $j(\lambda)$ of the reflected light, and downward with intensity $i(\lambda)$ of the incoming light. At a distance w above the substratum an infinitesimally thin layer of gel with spectral absorption coefficient $K(\lambda)$ and scattering coefficient $S(\lambda)$ satisfies the partial differential equations (Kang[4]).

$$\begin{aligned} -\partial i(\lambda)/\partial w(\lambda) &= -\big[K(\lambda)+S(\lambda)\big]i(\lambda)+S(\lambda)\,j(\lambda) \\ \partial j(\lambda)/\partial w(\lambda) &= -\big[K(\lambda)+S(\lambda)\big]j(\lambda)+S(\lambda)i(\lambda) \end{aligned} \qquad (2)$$

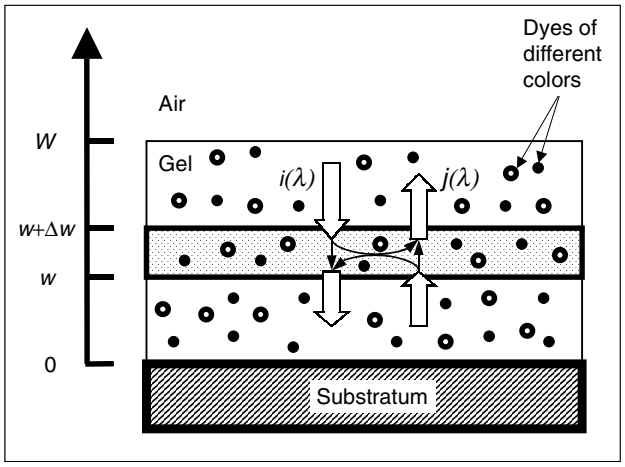

Figure 3. A simple model of photographic silver-halide paper consists of a gel layer with dyes and the paper as background (adapted from Kang[4]).

If $\Psi(\lambda,w) = j(\lambda)/i(\lambda)$ is the intensity ratio of reflected $j(\lambda)$ divided by incoming light $i(\lambda)$ at a certain distance w above the background medium and for a given wavelength λ, Eq. (2) becomes

$$\frac{\partial\Psi(\lambda,w)}{\partial w} = S(\lambda) - 2\big[K(\lambda)+S(\lambda)\big]\Psi(\lambda,w) + S(\lambda)\Psi^2(\lambda,w) \qquad (3)$$

For the following we assume that $S(\lambda)$ vanishes for all λ. At the boundary between the photographic gel and the underlying white background medium we assume a reflectivity $P_0(\lambda) = \Psi(\lambda,w=0)$. The modeled reflectivity of the photographic paper at the upper surface of the gel is labeled $P(\lambda) = \Psi(\lambda,w=W)$. For the absorption coefficient $K(\lambda)$ we then obtain (Berns[5])

$$K(\lambda) = -0.5\,\ln\left[\frac{P(\lambda)}{P_0(\lambda)}\right] \qquad (4)$$

Absorption coefficients refer to infinitesimal layers and are additive. At a given spot the total absorption coefficient $K(\lambda)$ equals the sum of the absorption coefficients $K_i(\lambda)$ for each dye. The relative absorption properties of each dye linearly scale with concentrations $c_i \in [0,1]$. Hence,

$$K(\lambda) = \sum_{i=1}^{i=n} c_i K_{i\,\max}(\lambda) \qquad (5)$$

where $K_{i\,\max}(\lambda)$ corresponds to the absorption coefficient of dye i with $c_i = 1$. Measured reflectance spectra $R(\lambda)$ suffer from internal scattering effects and include diffraction between the colored layer and the air. Saunderson [6] derived a semi-empirical formula to relate modeled spectra $P(\lambda)$ to measured spectra $R(\lambda)$.

$$P(\lambda) = \frac{R(\lambda) - f_{\mathrm{s}}}{1 - f_{\mathrm{s}} - f_{\mathrm{i}} + f_{\mathrm{i}}R(\lambda)} \qquad (6)$$

The above equation accounts for internal scattering (f_{i}) and scattering at the surface (f_{s}). For perfectly diffusing light the theoretically expected value for f_{i} is 0.614 (Williams and Clapper[7]). For our purpose f_{s} is negligibly small.

For the simplest model we need 4 reflectance spectra: A spectrum $R_i(\lambda)$ with i = 1, 2, 3 at maximal saturation for each of the primary dyes C, M, and Y, plus the reflectance spectrum $R_0(\lambda)$ of the white reference. The measured reflectance spectrum $R_0(\lambda)$ determines the scattering properties within the gel including the reflectance of the coated white background, when no dyes are present. In other words from $\mathrm{R}_0(\lambda)$ we can readily derive reflectivity $P_0(\lambda)$ using Eq. (6). Similarly from $R_i(\lambda)$ we can derive $P_{i\,\max}(\lambda)$ for the three primary dyes C, M, and Y. Eq. (4) then transforms $P_{i\,\max}(\lambda)$ to $K_{i\max}(\lambda)$. Once we know all the $K_{i\,\max}(\lambda)$ we can linearly combine dyes for an arbitrary set of dye concentrations c_i in the 'K-space' of absorption coefficients.

$$K(\lambda) = \big[1+\Delta(\lambda)\big]\cdot\sum_{i=1}^{i=n=3}(1+\Delta_i(\lambda))\cdot c_i K_{i\,\max}(\lambda) \qquad (7)$$

where – at least for the moment – $\Delta(\lambda) = 0$ and $\Delta_i(\lambda) = 0$ for all λ. Using the inverse Eq. (4) and (6) we obtain the reflectance spectrum $R(\lambda)$ of the dye mixture.

Reflectance spectra are convoluted with the color matching functions $x(\lambda)$, $y(\lambda)$, and $z(\lambda)$ of the CIE standard observer. The color matching function are designed to correspond to visual sensitivities. The convoluted spectra are weighted with the relative power spectrum of the light source $\Sigma(\lambda)$, and CIE tristimuli (X,Y,Z) are calculated. For $\Sigma(\lambda)$ we rely on the CIE D_{50} or D_{65} standard spectra.

$$N_X\int \mathrm{d}\lambda\; x(\lambda)R(\lambda)\Sigma(\lambda) \quad \text{with norm} \quad N_X = \frac{1}{\int \mathrm{d}\lambda\; x(\lambda)\Sigma(\lambda)} \qquad (8)$$

The remaining two coordinates Y and Z are computed accordingly. We may want to point out that the CIE color matching functions may be replaced by other kernels, for example to generate ANSI Status A densities. Starting with tristimuli (X,Y,Z) we use standard transformations to obtain the equivalent CIELAB color values (*cf* Giorgianni and Madden[1]).

Some explaining deserves the transition from normalized RGB device coordinates $\boldsymbol{p}_{RGB}$ to dye

concentrations c_i with i = 1 (C), 2 (M), and 3 (Y). By convention printer input (R,G,B) = (0,0,0) is equal to black with c_i = 1 for all i, and (R,G,B) = (1,1,1) corresponds to paper white with c_i = 0 for all i. The paper model has to be gray-calibrated in the same way as our printer. For a medium gray $\boldsymbol{p}_{RGB} = (R,G,B) = (\xi,\xi,\xi)$ with $\xi \in (0,1)$ we are looking for dye concentration $c(\xi) \in [0,1]$, so that the dye mixture with $c_1 = c_2 = c_3 = c$ results in a gray color with CIELAB value $L(\xi) = 100 \cdot \xi$. For RGB device coordinates $\boldsymbol{p}_{RGB}$ other than gray, each of the individual channels C, M, and Y are converted to the corresponding c_1, c_2, and c_3 concentrations, as if they were gray concentrations.

Even though the above set of definitions is unambiguous, we still have to solve a practical problem for colors near the black point. While the white reference yields $L(\xi=1) = 100$ by definition, the black point of any realistic photographic paper is always $L(\xi=0) = L_0 > 0$. Over the definition range [0,1] of RGB coordinates ξ, any reasonably behaved printing system is smooth and monotonous in $L(\xi)$. The definition range of $L(\xi)$ is $[L_0, 100] \subset [0, 100]$. To force $L(\xi)$ to reach 0 for the blackpoint a stretch function $f_{\text{stretch}}(\text{L})$ of some kind has to be applied to $L(\xi)$ with $\{L: L = f_{\text{stretch}}(L(\xi))\} = [0, 100]$.

Refined Paper Models

Our model – in the following referred to as *basic model* – is a surprisingly accurate description of silver-halide paper even at its simplest form. There are ample opportunities to refine the model. On one hand we could consider more layers and include additional physical processes. But we abandoned this approach, since it would introduce new, hard to define free parameters. A more heuristic approach is not to expand the model, but to fine-tune the input spectra. We measure additional colored patches and consider them corrections of higher order. The more patches we measure the more the model serves as a mere interpolation tool.

We relax the claim of Eq. (5). For the primary dyes C, M, and Y (i = 1, 2, 3) we now allow the absorption coefficient $K_i(\lambda)$ for dye concentrations $c_i \neq 1$ and $c_i \neq 0$ to slightly deviate from $c_i K_{i\,\max}(\lambda)$. Mathematically these deviations are expressed in form of 'delta functions'

$$\Delta_i(\lambda) = \frac{K_i(\lambda)}{c_i \cdot K_{i\,\max}(\lambda)} - 1 \qquad (9)$$

These $\Delta_i(\lambda)$ are supplied to Eq. (7) and guarantee that the C-, M-, and Y- axis exactly match the measurements. In reality we can only get an approximation of $\Delta_i(\lambda)$. We measure a few colored C, M, and Y patches at different saturation levels and estimate $\Delta_i(\lambda)$ with a 'damped' cubic-spline interpolation.

Using Eq. (9) we have unlimited means to improve the model predictions for the three primary dyes C, M, and Y. The largest discrepancies now occur for dye mixtures far away from the primary color axis of C, M, and Y. It seems obvious to obtain additional measurements in these critical areas in between the primary color axis. These measurements are compared with the model predictions of the $\Delta_i(\lambda)$-corrected paper model. The differences $\Delta(\lambda)$ are second-order corrections and are computed in analogy to Eq. (9). In Eq. (7) they are factored in *after* the absorption coefficients of the primary dyes have been co-added.

We developed a color chart with 28 colored patches. Spectra are measured from 16 colored patches along the C-, M-, Y-, and gray-axis. The measurements are taken at different levels of saturation with at least one patch at maximal saturation. On the gray axis paper white is an additional mandatory field. The color chart also contains 4 reddish colors with printer coordinates $\boldsymbol{p}_{RGB} = (R,G,B)$ = (1,0,0), (1,0,½), (1,½,0), and (1,½,½). Through permutations of the coefficients we obtain 2×4 additional color patches that lie in the greenish and bluish color range.

The three primary dyes C, M, and Y can be considered ortho-normal base vectors of a linear space. Any other triplet of base vectors is a viable replacement of the CMY vectors. Since the human eye is extremely sensitive to the slightest departures from neutral gray, we declare the gray-axis one of our base vectors. For a given triplet of CMY concentrations $(c_1, c_2, c_3) = (c_{\text{C}}, c_{\text{M}}, c_{\text{Y}})$, the gray concentration c_{Gray} is defined by

$$c_{\text{Gray}} = \min(c_{\text{C}}, c_{\text{M}}, c_{\text{Y}}) \qquad (10)$$

In the gray-removed color triplet $(c_1 - c_{\text{Gray}}, c_2 - c_{\text{Gray}}, c_3 - c_{\text{Gray}})$ at least one of the three coefficients equals 0. The remaining, non-zero coefficients span a 2-dimensional color plane. If the first coefficient vanishes, then the plane connects M, Y, and R. Similarly we find a plane through colors C, Y, G or C, M, B, if the second or third coefficient turns zero. Assuming the two non-zero, gray-removed components are denoted c_{a} and c_{b}, the red, green, or blue component c_{RGB} becomes

$$c_{\text{RGB}} = \min(c_{\text{a}}, c_{\text{b}}) \qquad (11)$$

Again one of the two coefficients $(c_{\text{a}} - c_{\text{RGB}}, c_{\text{b}} - c_{\text{RGB}})$ will be 0. The non-zero coefficient determines concentration c_{CMY} of the residual C, M, or Y component.

Summarizing the above algorithm produces a triplet of concentrations $(c_{\text{Gray}}, c_{\text{RGB}}, c_{\text{CMY}})$. Starting with the set of 7 base colors {Gray, R, G, B, C, M, Y} we select dye gray. Then, depending on the outcome of the above algorithm, we grab one color from triplet {R, G, B} and one color from triplet {C, M, Y}. Finally from our color chart of 28 patches we gather the necessary information to run the $\Delta(\lambda)$- and $\Delta_i(\lambda)$-corrected paper model.

We tested three models: The basic CMY model (A), a $\Delta_i(\lambda)$-corrected CMY model (B), and the model with 28 patches (C). We examined four different paper brands: Kodak™ Royal Edge 8 (Kodak), Kodak™ Supra III (Kodak prof.), Fuji™ Crystal Archive (Fuji), and Agfa™ Paper 11 (Agfa). A color chart with 420 fields was measured that roughly sampled the RGB space of the printer. The CIELAB values were determined with a GretagMacbeth™ Spectroscan spectrometer. The estimated, cumulative 1σ-error of a single measurement is approximately $\Delta E \approx 1$. Table 1 summarizes the result for the various models. Listed are the averaged and maximal difference ΔE between calculation and actual print analyzing all 420 fields.

Table 1. Paper Models in Comparison.

	Model (A)	Model (B)	Model C
Kodak			
ΔE average	4.88	2.71	2.63
ΔE max	11.76	8.35	8.95
Kodak prof.	4.36	2.93	2.53
ΔE average	10.63	9.51	7.68
ΔE max			
Fuji			
ΔE average	4.02	3.87	3.21
ΔE max	13.86	14.24	11.18
Agfa			
ΔE average	3.45	2.99	2.33
ΔE max	9.60	7.91	8.53

Discussion

The various elements of our paper model are helpful in a number of different places.

1. At the input to connect film densities $\boldsymbol{d}_{\text{film}}$ to device coordinates $\boldsymbol{p}_{\text{RGB}}$ of the printer, and to relate $\boldsymbol{p}_{\text{RGB}}$ to the resulting CIELAB color values of a virtual photographic paper (*cf* Fig. 1 and 2).
2. At the output to profile silver-halide paper on the basis of a very small color chart (*cf* Fig. 2).
3. To improve the robustness and to speed up the iteration process during calibration (Zolliker [3]).

1. $\boldsymbol{d}_{\text{film}} \rightarrow \boldsymbol{p}_{\text{RGB}} \rightarrow$ CIELAB

We introduced an idealized saturation curve for photographic paper to transform universal RGB film densities $\boldsymbol{d}_{\text{film}}$ to device coordinates $\boldsymbol{p}_{\text{RGB}}$ of the printer. For a real paper we demonstrated how the resulting CIELAB color value can be predicted for a given RGB printer input $\boldsymbol{p}_{\text{RGB}}$. The difficulty with the data path from negative film to paper lies in the fact that both $\boldsymbol{d}_{\text{film}}$ and $\boldsymbol{p}_{\text{RGB}}$ are artificial quantities. They describe an imaginary film and an imaginary paper, respectively.

But most of all we need to specify suitable reflectance spectra $R_i(\lambda)$ for the conversion from printer coordinates $\boldsymbol{p}_{\text{RGB}}$ to the CIELAB color space. Reasonable results can be achieved, if we feed the basic model with measured CMY spectra of a commercially available paper. Unfortunately reflectance spectra $R_i(\lambda)$ of a concrete paper have one major disadvantage. We risk to unnecessarily limit the gamut of the print. This can happen, if at the output we map the CIELAB image onto a different target paper than we used for the spectra $R_i(\lambda)$ at the input. This dilemma led us to the concept of a 'super-paper'. The gamut of this ideal paper attempts to embrace the gamut of all real photographic paper. The extended gamut has to remain paper-like and the out-of gamut areas must be kept at a reasonable size. Otherwise the gamut mapping process is forced to compromise too much in the out of gamut zones with the effect that we start loosing contours in highly saturated colors. One way to generate an ideal paper is to determine averaged CMY spectra from a large set of different paper brands. To increase the gamut the color saturation of these averaged spectra is stretched by a certain amount. Digital output is usually in sRGB. Another important sRGB output channel is the CRT monitor. The gamut of the sRGB color space is drastically different from the typical gamut of silver-halide paper (Fig. 4). To aid with gamut mapping to the two major output color spaces – the color space of the print and the sRGB color space – spectra $R_i(\lambda)$ turned out to be a good choice, if they meet two conditions: They have a gamut larger than any real paper, and their gamut fills a large fraction of the sRGB space.

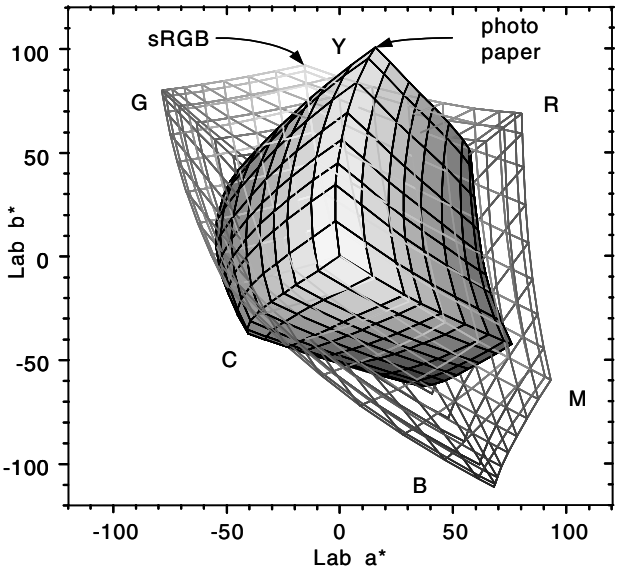

Figure 4. The gamut of sRGB in comparison with the gamut of a typical paper (from Heimgartner et al. [8]).

2. Profiling with a Small Color Chart

For output profiling classical color management tools use a large (≥ 200) set of colored patches to probe the gamut of the output device and to relate CIELAB color values to the corresponding printer RGB values. With a spectral model we need less measurements (between 4 to ~30), and we can determine the gamut boundaries more accurately. A model is also far less vulnerable to discontinuities in color gradients than the empirical method of standard profiling tools.

In the section on 'refined paper models' we showed how we can accurately describe a real paper on the basis of 28 colored patches. Profiling to an output device includes gamut mapping and a conversion from CIELAB coordinates to printer device coordinates $\boldsymbol{p}_{\text{RGB}}$. The former requires the knowledge of the gamut boundaries. If we insert RGB coordinates on the surface of the RGB cube the paper model directly returns the CIELAB values of the gamut boundaries. The mapping process itself is a function within the CIELAB color space that maps *(L,a,b)* to *(L',a',b')*. Our spectral paper model delivers CIELAB values for a given set of RGB printer values $\boldsymbol{p}_{\text{RGB}}$. The function $f(\boldsymbol{p}_{\text{RGB}}) = (L,a,b)$: $\Re^3 \rightarrow \Re^3$ can be inverted using a multidimensional polynomial least-square fit. The inverse $f^{-1}(L',a',b')$ maps *(L',a',b')* triplets within the gamut to corresponding $\boldsymbol{p}_{\text{RGB}}$ coordinates, the destination space of the output profile.

3 Efficient Gray Calibration

A paper model can increase the robustness and decrease the number of iterations of the gray calibration (Zolliker[3]).

Conclusions

We presented a paper model to simulate the color reproduction of silver-halide paper. The model mainly consists of two elements. A paper saturation curve and a one parameter Kubelka-Munk model for color mixing. The model is used to determine CIELAB color values from film densities, to generate high-quality printer profiles on the basis of a very small color chart, and to improve the gray calibration of the printer.

References

1. E. J. Giorgianni and T. E. Madden, Digital Color Management – Encoding Solutions, Addison Wesley Longman, MA, 1997.
2. G. Marbach, W. Kraft, and P. Zolliker, EyeTech Scanning in Hybrid and Digital Printers of Gretag Imaging, Proc, IS&T, pg. 17 (2000).
3. P. Zolliker, „Fast Gray Calibration for Digital Photographic Printers“, paper presented at CGIV'2002 (2002).
4. H. R. Kang, Color Technology for Electronic Imaging Devices, SPIE, WA, 1997, pg. 48.
5. R. S. Berns, J. Electron Imag. 2, 359 (1993).
6. J. L. Saunderson, J. Opt. Soc. Am. 32, 727 (1942).
7. F. C. Williams and F. R. Clapper, J. Opt. Soc. Am. 43, 595 (1953).
8. E. Heimgartner, P. Zolliker, and R. Meier, Color Management in Gretag's Digital Systems Cyra and MasterflexD 1008, paper presented at IS&T 2002 (2002).

Biographies

Roland Meier received his PhD in Experimental Physics from the University of Bern in 1992. From 1994 to 1996 he was a post-doctoral fellow at the University of Maryland. From 1996 to 1999 he held a Hubble Space Telescope NICMOS (IR spectrograph) fellowship at the Institute for Astronomy at the University of Hawaii. In 2000 he was a recipient of the Zeldovic medal issued by COSPAR and the Russian Academy of Sciences. In January 2000 he joined the R&D team at Gretag Imaging, where he is mainly working on image quality and color management issues.

Peter Zolliker has a degree in Physics from the Swiss Federal Institute of Technology and received a Ph.D. in Crystallography from the University of Geneva in 1987. From 1987 to 1988 he was a post-doctoral fellow at the Brookhaven National Laboratory, New York. In 1989 he joined the R&D team at Gretag Imaging. His work is mainly focussed on image analysis, image quality and setup and color management procedures for digital printers.